Valley currents and nonlocal resistances of graphene nanostructures with broken inversion symmetry from the perspective of scattering theory

George Kirczenow*
Department of Physics, Simon Fraser University, Burnaby, British Columbia, Canada V5A 1S6
(Received 30 June 2015; published 17 September 2015)

Valley currents and nonlocal resistances of graphene nanostructures with broken inversion symmetry are considered theoretically in the linear response regime. Scattering state wave functions of electrons entering the nanostructure from the contacts represented by groups of ideal leads are calculated by solving the Lippmann-Schwinger equation and are projected onto the valley state subspaces to obtain the valley velocity fields and total valley currents in the nanostructures. In the tunneling regime when the Fermi energy is in the spectral gap around the Dirac point energy, inversion symmetry breaking is found to result in strong enhancement of the nonlocal four-terminal Büttiker-Landauer resistance and in valley currents several times stronger than the conventional electric current. These strong valley currents are the direct result of the injection of electrons from a contact into the graphene in the tunneling regime. They are chiral and occur near contacts from which electrons are injected into the nanostructure whether or not a net electric current flows through the contact. It is also pointed out that enhanced nonlocal resistances in the linear response regime are not a signature of valley currents arising from the combined effect of the electric field and Berry curvature on the velocities of electrons.

DOI: 10.1103/PhysRevB.92.125425 PACS number(s): 72.80.Vp, 73.63.−b, 73.63.Rt

I. INTRODUCTION

Graphene is a single atomic layer of carbon atoms arranged on a honeycomb lattice. Since the early work of Wallace [1], it has been known that the electronic energy bands of graphene near the Fermi energy take the form of a degenerate pair of cones, also referred to as "valleys." The electronic density of states of graphene vanishes at the Dirac point energy which coincides with the Fermi energy in pristine graphene. More recently, it was recognized that the electronic structure of graphene has topological properties that relate to the Berry phase and Berry curvature [2]. Specifically, graphene has a nonzero Berry phase associated with closed paths in reciprocal space that enclose a valley apex [3]. If the inversion symmetry of the graphene lattice is broken, for example, by a staggered potential at the two atoms of the unit cell, then the Berry curvature $\Omega_{\mathbf{k}}$ becomes nonvanishing near the apex of each valley [4]. In semiclassical theories of electron transport in graphene, the electron velocity $\mathbf{v}_{\mathbf{k}}$ is related to the Berry curvature by [2,5–8]

$$\mathbf{v}_{\mathbf{k}} = \frac{1}{\hbar}\frac{\partial \epsilon_{\mathbf{k}}}{\partial \mathbf{k}} + \dot{\mathbf{k}} \times \Omega_{\mathbf{k}}, \tag{1}$$

where $\epsilon_{\mathbf{k}}$ is the energy of a Bloch state with wave vector $\mathbf{k}$ and, in the absence of magnetic fields,

$$\hbar\dot{\mathbf{k}} = q_e\mathbf{E}, \tag{2}$$

where q_e is the electron charge and $\mathbf{E}$ is the electric field. Since $\Omega_{\mathbf{k}}$ points in opposite directions in the two valleys, Eqs. (1) and (2) imply that, in the presence of an electric field $\mathbf{E}$, electrons in the two valleys of graphene with broken inversion symmetry will have differing velocities. This difference in velocity might, in principle, be used to separate electrons belonging to the different valleys spatially, and thus be employed in future valleytronic devices in which the valley index of electrons plays a role somewhat analogous to that of the electron-spin quantum number in spintronic devices.

Recently, Gorbachev *et al.* [9] carried out nonlocal four-terminal resistance measurements on graphene placed on a hexagonal boron nitride (hBN) substrate, varying the graphene Fermi level by the application of a gate voltage. They found a striking enhancement of the measured nonlocal resistance when the Fermi level passed through Dirac points for samples with the crystallographic axes of the graphene aligned with those of the hBN. They interpreted the enhanced nonlocal resistance as a signature of valley currents in their samples based on the following intuitive picture [9]: The aligned hBN substrate breaks the inversion symmetry of graphene [10–13]. This results in nonzero Berry curvatures for states close in energy to Dirac points. Then, according to Eqs. (1) and (2), an electric field $\mathbf{E}$ that drives electric current through the sample would result in differing electron velocities in the two graphene valleys. This would imply a net valley current transverse to the electric current when the Fermi level is close to a Dirac point energy [9]. It was further argued [9] that this valley current flows into the region of the sample between the voltage probes and induces an electric field there, resulting in a potential difference between the voltage probes and an enhancement of the nonlocal resistance, consistent with the experiment [9].

However, valley currents were not observed *directly* in the experiment of Gorbachev *et al.* [9]. Also, the interaction between the hBN and graphene is expected theoretically [10–13] to open an energy gap in the electronic density of states of graphene around the Dirac point energy, where the Fermi level is located when the observed [9] enhanced nonlocal resistance has its maximum value. The presence of this gap is supported by the observation of activated transport by Gorbachev *et al.* [9] in some of their samples. Within the gap the transport mechanism is quantum tunneling, a phenomenon that has no classical analog. Therefore, the applicability of the semiclassical Eqs. (1) and (2) to this regime is unclear and a fully quantum mechanical theory of transport is necessary.

*kirczeno@sfu.ca

A rigorous, fully quantum mechanical approach to calculations of multiterminal transport coefficients of nanostructures is provided by Büttiker-Landauer theory [14]. However, the conceptual framework of Büttiker-Landauer theory differs from that of the topological arguments [9] that have been outlined above. For example, within Büttiker-Landauer theory, in the linear response regime (i.e., in the limit where the applied bias voltages and currents approach zero), the four-terminal resistances depend only on the set of quantum electron transmission probabilities $\{T_{i,j}\}$ between all pairs of contacts $\{i,j\}$ and the reflection probabilities $\{R_{i,i}\}$ at contacts $\{i\}$ evaluated at the Fermi energy (or, at finite temperatures, at energies near the Fermi energy). In this limit, the electric field $\mathbf{E}$ that appears in Eq. (2) goes to zero, and therefore in this limit it has no effect on $\{T_{i,j}\}$ and $\{R_{i,i}\}$. Therefore, according to Büttiker-Landauer theory, the topological mechanism of valley currents that is embodied in the term $\dot{\mathbf{k}} \times \Omega_{\mathbf{k}}$ in Eq. (1) has *no* effect on four-terminal resistances (or, more generally, on two-, three-, or other multiterminal resistances, including nonlocal resistances) in the linear response regime. Thus it follows from Büttiker-Landauer theory that nonlocal resistance measurements in the linear response regime cannot provide experimental evidence of topological effects arising from the electric field in Eq. (2).

In other words, Büttiker-Landauer theory shows that nonlocal (and other) resistances measured in the linear response regime do not depend on whether electrons travel through the sample under the influence of an electric field due to applied bias voltages or simply scatter through the sample freely in the energy window between the highest and lowest contact electrochemical potentials without being subjected to any driving electric field. This means that the effects of the topological term $\dot{\mathbf{k}} \times \Omega_{\mathbf{k}}$ in Eq. (1) that arise from the driving electric field cannot be detected by local or nonlocal resistance measurements in the linear response regime.

It is therefore of interest to explore theoretically the multiterminal resistances and valley currents in fully quantum mechanical models of graphene devices with broken inversion symmetry from the perspective of Büttiker-Landauer theory. This is done in the present paper for transport in graphene nanostructures subjected to staggered potentials in the linear response regime. It will be shown here that the application of a staggered potential results in strong enhancement of the nonlocal four-terminal resistance when the Fermi level is close to the Dirac point energy, in qualitative agreement with the experimental findings of Gorbachev *et al.* [9]. Despite the studied nanostructures having atomically abrupt boundaries where electrons scatter strongly and crystal momentum is not conserved, valley currents, up to several times larger than the conventional electric current, will be shown to appear in response to electrochemical potential differences between the electrodes when the Fermi level is near the Dirac point of graphene nanostructures with broken inversion symmetry. These large valley currents are not generated by the topological mechanism embodied in Eqs. (1) and (2) since the present calculations are in the linear response limit where the driving electric field $\mathbf{E}$ in Eq. (2) tends to zero and therefore it does not appear in the Hamiltonian of the system in these Büttiker-Landauer-theory-based calculations. Because these strong valley currents occur in a gap in the energy spectrum of the nanostructure, they require electron tunneling and consequently their strength decays rapidly as the distance from a contact that injects electrons into the graphene nanostructure increases. These valley currents will be seen to be chiral and to travel along the edge of the graphene that is in contact with an electrode that injects electrons into the graphene. If electrons are injected into the graphene nanostructure with broken inversion symmetry from a scanning tunneling microscope (STM) tip, the valley currents will be shown to form a vortex circulating around the location at which the electron injection occurs. At Fermi energies further from the Dirac point and outside of the gap in the density of states of the nanostructure, valley currents are also induced by bias voltages applied to the nanostructure. However, in this regime they are found to be weaker, not to require inversion symmetry breaking, and to extend into regions of the nanostructure that are not close to the contacts.

The remainder of this paper is organized as follows. In Sec. II, the model of graphene nanostructures with broken inversion symmetry coupled to current and voltage contacts that is studied in this work is presented. Büttiker-Landauer theory and the Lippmann-Schwinger equation and how they apply to this model are outlined. Valley currents, valley velocity fields, and nonlocal resistances are defined and the methodology used to calculate them is described. The numerical results obtained from these calculations are presented in Sec. III. The significance of the present findings is discussed in Sec. IV.

II. MODEL AND FORMALISM

In this paper, the graphene nanostructures will be described by the standard nearest-neighbor tight-binding Hamiltonian on a honeycomb lattice,

$$H_{\mathrm{GN}} = \sum_n \epsilon_n a_n^\dagger a_n - \sum_{\langle n,m \rangle} t_{nm}(a_n^\dagger a_m + \mathrm{H.c.}), \qquad (3)$$

where ϵ_n is the on-site energy, $t_{nm} = t = 2.7$ eV defines the matrix element between p_z orbitals on nearest-neighbor atoms, and the spin index is suppressed. This Hamiltonian with $\epsilon_n = 0$ is known to describe the π-band dispersion of graphene well at low energies [15], and has been used in numerous studies of electron transport in graphene nanostructures [16]. In order to introduce inversion symmetry breaking into the model, the simple choice $\epsilon_n = \pm\Delta$ is made so that ϵ_n is positive on one atom of the graphene unit cell and negative on the other. The amplitude of the symmetry-breaking energy is chosen to be $\Delta = 0.0602$ eV, consistent with estimates for graphene on hBN reported in Ref. [11].

This idealized model has been chosen since the purpose of this paper is to investigate the fundamental effects of inversion symmetry breaking in its simplest form on multiterminal transport coefficients and valley currents within the fully quantum mechanical Büttiker-Landauer framework. It should be noted that the graphene on the hBN system is more involved since the lattice parameters of hBN and graphene have a 2% mismatch and local configurations with N atoms under the centers of graphene hexagons and B atoms under C atoms have the lowest energy [11]. However, these complications will not be considered here.

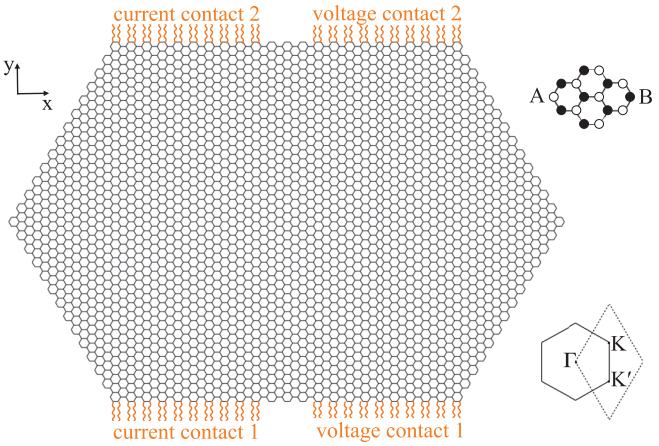

FIG. 1. (Color online) Graphene nanostructure with armchair edges. The size of the nanostructure in the y direction is 9.838 nm. Electron stream is injected through current contact 1 and exits through current contact 2. There is no net electric current entering or leaving through the voltage contacts 1 and 2; the potential difference between them is measured. Wavy lines represent ideal semi-infinite 1D leads connecting graphene C atoms to electron reservoirs. Upper right inset: The graphene sublattices A (B) = open (filled) circles. Lower right inset: Hexagonal (solid) and rhombic (dotted) Brillouin zones of graphene. K and K' are the two Dirac points.

In Büttiker-Landauer theory [14], at zero temperature and in the linear response regime, the currents I_i flowing towards the nanostructure in contacts i are related to the electrochemical potentials μ_i of the contacts by

$$I_i = \frac{q_e}{h}\left(N_i\mu_i - \sum_j T_{i,j}\mu_j\right), \tag{4}$$

where N_i is the number of electronic modes incident on the nanostructure from contact i and $T_{i,j}$ is the multichannel electron transmission probability from contact j to contact i. $T_{i,i} = R_{i,i}$ is the multichannel electron reflection probability from the nanostructure in contact i.

The coefficients $T_{i,j}$ that enter the Büttiker-Landauer theory are calculated in this paper as in many previous theoretical studies of quantum transport in nanostructures [17–30] with semiconducting [19–21,23,29], molecular [17–28,30], metallic [17–30], magnetic [23,25,28,29], and carbon-based [28] constituents. Each contact is represented by a set of ideal semi-infinite one-dimensional (1D) tight-binding leads (the wavy lines in Fig. 1) with one orbital per site and nearest-neighbor hopping. One such ideal lead is attached to each peripheral site of the graphene nanostructure that is adjacent to a contact. The Hamiltonian of lead n is

$$H_{\mathrm{L}n} = \sum_r \epsilon_n b_r^\dagger b_r - \sum_{\langle r,s\rangle} t(b_r^\dagger b_s + \mathrm{H.c.}), \tag{5}$$

where t is the same as in H_{GN} [Eq. (3)]. The site energy ϵ_n in Eq. (5) is the same as that of the site of the graphene nanostructure to which the lead is connected. The coupling Hamiltonian between lead n and the edge site of the graphene nanostructure is

$$W_n = -t(b_n^\dagger a_n + \mathrm{H.c.}). \tag{6}$$

The quantum transmission amplitudes for an electron to scatter at energy E via the nanostructure from one 1D ideal lead to another are found by solving the Lippmann-Schwinger equation,

$$|\psi^m\rangle = \left|\phi_0^m\right\rangle + G_0(E)W|\psi^m\rangle\ , \tag{7}$$

where $|\phi_0^m\rangle$ is an electron eigenstate of the m^{th} ideal semi-infinite lead that is decoupled from the graphene nanostructure, $G_0(E)$ is the Green's function of the decoupled system of the ideal leads and the graphene nanostructure, and $W = \sum_n W_n$ is the coupling between the graphene nanostructure and the ideal leads. $|\psi^m\rangle$ is the scattering eigenstate of the complete coupled system associated with the incident electron state $|\phi_0^m\rangle$. Then,

$$T_{i,j}(E) = \sum_{n,m} \left|t_{nm}^{ij}(E)\right|^2 v_n^i/v_m^j, \tag{8}$$

where $t_{nm}^{ij}(E)$ is the quantum transmission amplitude [obtained from the scattering state $|\psi^m\rangle$ defined by Eq. (7)] for an electron at energy E to scatter via the graphene nanostructure from ideal 1D lead m of contact j to ideal 1D lead n of contact i. The sum is over ideal leads n (m) in contact i (j). $v_{n(m)}^{i(j)}$ is the electron velocity in ideal 1D lead n (m) of contact i (j) at energy E; $v_n^i = \frac{1}{\hbar}\frac{\partial\epsilon}{\partial k}$ where ϵ are the energy eigenvalues of the Hamiltonian $H_{\mathrm{L}n}$ [Eq. (5)] of an infinite ideal 1D tight-binding chain.

Having evaluated $T_{i,j}$ at the Fermi energy in this way, the Büttiker equations (4) are solved in the linear response regime to find the nonlocal four-terminal resistance,

$$R_{\mathrm{NL}} = \Delta V/I, \tag{9}$$

where I is the current passing through the current contacts and $\Delta V = \Delta\mu/q_e$ is the potential difference between the voltage contacts; see the contacts in Fig. 1.

The valley currents induced in the nanostructure in response to to the electrochemical potential differences between the various contacts in the linear response regime are estimated as follows: The scattering state $|\psi^m\rangle$ of electrons injected into the nanostructure from ideal 1D lead m is calculated at the Fermi energy for every lead m by solving the Lippmann-Schwinger equation (7). Then the scattering state $|\psi^m\rangle$ is projected onto the subspaces of Bloch states of graphene that belong to the K and K' valleys. This yields the projected valley states, $|\psi_K^m\rangle$ and $|\psi_{K'}^m\rangle$, respectively. For this purpose, a Bloch state is assigned to the K (K') valley if its wave vector lies within the upper (lower) half of the rhombic Brillouin zone defined by the dotted boundary in the lower right inset of Fig. 1.

The ξ component of the velocity operator for electrons within the graphene nanostructure is

$$v_\xi = \frac{1}{i\hbar}[\xi, H_{\mathrm{GN}}], \tag{10}$$

where $\xi = \sum_p \xi_p a_p^\dagger a_p$, and ξ_p is the ξ coordinate of atomic site p of the graphene nanostructure. The expectation value of v_ξ in the graphene nanostructure in the state $|\psi^m\rangle$ is then

$$\langle\psi^m|v_\xi|\psi^m\rangle = \frac{it}{2\hbar}\sum_{k,l}(\xi_k - \xi_l)\left(\psi_k^{m*}\psi_l^m - \psi_k^m\psi_l^{m*}\right), \tag{11}$$

where k and l are nearest-neighbor sites of the graphene nanostructure, $\xi_l = x_l$ or y_l, $\psi_l^m = \langle Z_l|\psi^m\rangle$, and $|Z_l\rangle$ is the $2p_z$ orbital of the carbon atom at site l.

For a graphene nanostructure with multiple contacts i each at its own electrochemical potential μ_i, the electron transport through the device is governed by a weighted average over the velocities associated with the scattering states injected by the various ideal leads m_i that make up all of the contacts i. The relevant weighted average will be defined here as

$$v_\xi = \sum_{m,i}\langle\psi^{m_i}|v_\xi|\psi^{m_i}\rangle\Delta\mu_i \Big/ \sum_{m,i}\Delta\mu_i, \tag{12}$$

where $\Delta\mu_i = \mu_i - \mu_{\min}$, and $\mu_{\min}$ is the electrochemical potential of the contact with the lowest electrochemical potential.

The weighted valley velocities $v_{K\xi}$ and $v_{K'\xi}$ for electrons in valleys K and K' are defined similarly by replacing $|\psi^m\rangle$ and $|\psi^{m_i}\rangle$ in Eqs. (11) and (12) by their projections $|\psi_K^m\rangle$ and $|\psi_K^{m_i}\rangle$, and $|\psi_{K'}^m\rangle$ and $|\psi_{K'}^{m_i}\rangle$ onto the valleys K and K', respectively. The weighted valley velocity is then defined as

$$v_\xi^{\rm val} = (v_{K\xi} - v_{K'\xi}). \tag{13}$$

Equation (11) expresses the expectation value of the electron velocity as a sum of terms evaluated at pairs (k,l) of nearest-neighbor atoms of the graphene nanostructure. This suggests that each such term be interpreted as the value of the velocity field for the scattering state $|\psi^m\rangle$ at the location of each nearest-neighbor pair. Assigning this value of the velocity field $v_\xi^{\rm F}$ arbitrarily to the midpoint $(x,y) = [(x_k + x_l)/2,(y_k + y_l)/2]$ of the atomic pair yields

$$\langle\psi^m|v_\xi^{\rm F}(x,y)|\psi^m\rangle = \frac{it}{\hbar}(\xi_k - \xi_l)\left(\psi_k^{m*}\psi_l^m - \psi_k^m\psi_l^{m*}\right). \tag{14}$$

The corresponding velocity field weighted by the contributions of the states contributing to transport through the nanostructure is then, as in Eq. (12), given by

$$v_\xi^{\rm F}(x,y) = \sum_{m,i}\langle\psi^{m_i}|v_\xi^{\rm F}(x,y)|\psi^{m_i}\rangle\Delta\mu_i \Big/ \sum_{m,i}\Delta\mu_i. \tag{15}$$

Obtaining the weighted velocity fields $v_{K\xi}^{\rm F}$ and $v_{K'\xi}^{\rm F}$ for the valleys K and K' similarly by replacing $|\psi^m\rangle$ by the projections $|\psi_K^m\rangle$ and $|\psi_{K'}^m\rangle$, the valley velocity field is defined as

$$v_\xi^{\rm val\,F}(x,y) = v_{K\xi}^{\rm F}(x,y) - v_{K'\xi}^{\rm F}(x,y). \tag{16}$$

III. RESULTS

The results of Büttiker-Landauer calculations of the nonlocal four-terminal resistance $R_{\rm NL}$ defined by Eq. (9) for the structure in Fig. 1 at zero temperature in the linear response regime are shown in Fig. 2(a) as a function of the Fermi energy $E_{\rm F}$. The Fermi level crosses the Dirac point energy at $E_{\rm F} = 0$. Near the Dirac point, $R_{\rm NL}$ for the model with $\Delta = 0.0602$ eV (orange line) exceeds $R_{\rm NL}$ for $\Delta = 0$ (black line) by a factor of $\sim$2.5. Thus, within Büttiker-Landauer theory, the breaking of inversion symmetry of the graphene unit cell results in strong enhancement of the nonlocal resistance near the Dirac point. However, as can also be seen in Fig. 2(a), well away from the Dirac point energy the inversion symmetry breaking has little effect on the nonlocal resistance.

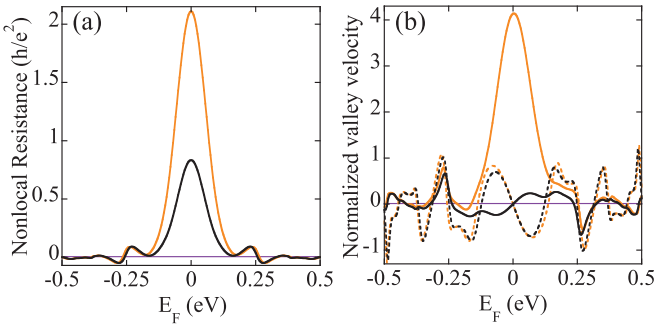

FIG. 2. (Color online) Calculated linear response properties vs Fermi energy of the structure in Fig. 1 at zero temperature. Current I flows through the current contacts with no net current through either voltage contact. Results for symmetry-breaking parameter $\Delta = 0.0602$ (0.0) eV are orange (black). (a) Nonlocal resistance $R_{\rm NL}$ [Eq. (9)]. (b) Normalized valley velocities $v_x^{\rm val}/v_y$ and $v_y^{\rm val}/v_y$ [Eqs. (12) and (13)] are solid and dashed lines, respectively.

Since the net electron flow in the structure in Fig. 1 is from current contact 1 to current contact 2 (i.e., in the y direction), the weighted velocity vector $\vec{v}$ [Eq. (12)] is expected to point in the y direction. Accordingly, v_x in Eq. (12) is found to be zero within numerical error in the present computations. The computed normalized, weighted valley velocities $v_x^{\rm val}/v_y$ and $v_y^{\rm val}/v_y$ are shown in Fig. 2(b). They are found to be nonzero except at isolated values of the Fermi energy, both in the presence and absence of symmetry breaking. Note that $v_\xi^{\rm val}/v_y = I_\xi^{\rm val}/I$, where $I_\xi^{\rm val}$ is the ξ component of the valley current and I is the total electric current through the nanostructure. The most striking feature of Fig. 2(b) is the strong peak near the Dirac point ($E_{\rm F} = 0$) of $v_x^{\rm val}/v_y = I_x^{\rm val}/I$ for broken inversion symmetry (the solid orange curve). At its maximum, the valley current in the x direction exceeds the total conventional electric current through the nanostructure by a factor of more than 4. This peak of the valley current is in the gap (of width 0.264 eV) in the energy spectrum of the broken symmetry nanostructure around the Dirac point. By contrast, the x component of the valley current in the absence of symmetry breaking (solid black curve) and the y component of the valley current with (orange dashed curve) and without (black dashed curve) symmetry breaking all vanish at the Dirac point and are relatively weak elsewhere. As can also be seen in Fig. 2(b), for $E_{\rm F}$ well away from the Dirac point energy, both $v_x^{\rm val}/v_y$ and $v_y^{\rm val}/v_y$ are insensitive to the breaking of the inversion symmetry of the graphene.

The full widths of the central peaks of both the nonlocal resistance and the normalized valley velocity $v_x^{\rm val}/v_y$ for the system with broken inversion symmetry [the orange curves in Figs. 2(a) and 2(b), respectively] are close in size to the 0.264 eV gap in the energy spectrum of the broken-symmetry nanostructure. Because the value of the symmetry-breaking parameter is relatively small ($\Delta = 0.0602$ eV), the size of the spectral gap is determined mainly by the quantum confinement of the electrons in the graphene nanostructure and the armchair character of the nanostructure's edges [16]. Thus for the same nanostructure but with the symmetry breaking turned off ($\Delta = 0$), the width of the energy gap has a similar value, 0.235 eV. For this reason, the main nonlocal resistance peak in Fig. 2(a)

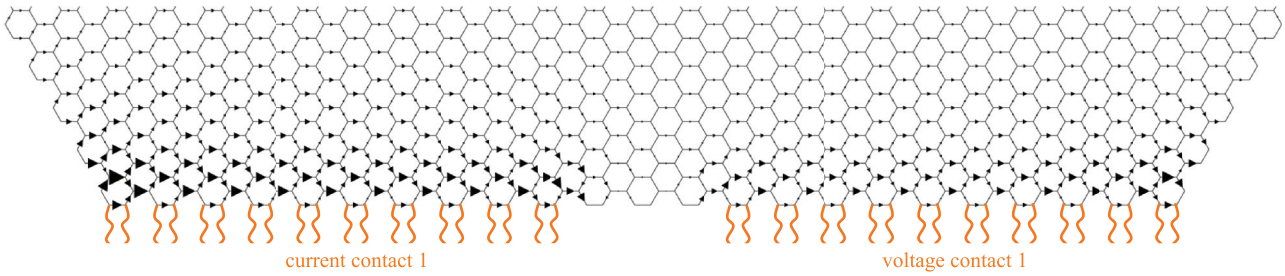

FIG. 3. (Color online) Valley velocity field [Eq. (16)] in the lower part of the structure in Fig. 1 for electron flow from current contact 1 to current contact 2 (shown in Fig. 1). For electron flow in this direction, the valley velocity field is much stronger in the vicinity of the contacts shown here than elsewhere in the graphene nanostructure. $\Delta = 0.0602$ eV. $E_F = 0$.

has almost the same width for $\Delta = 0$ (black curve) as for $\Delta = 0.0602$ eV (orange curve).

The valley velocity field $\vec{v}^{\,\mathrm{val\,F}}(x,y)$ is shown in Fig. 3 for the lower part of the nanostructure in Fig. 1. Inversion symmetry is broken and the Fermi level is at the Dirac point. The valley velocity is large near current contact 1 and voltage contact 1. Its magnitude initially increases, but then decreases rapidly with increasing distance from the contacts. The valley velocity is clearly chiral, pointing mainly from left to right near the graphene boundary shown (its overall direction reverses if the sign of Δ, the symmetry-breaking parameter, is changed), but it does not extend along the boundary much beyond where a contact ends.

In Fig. 3, the electron flow enters the graphene nanostructure through current contact 1 and exits through current contact 2 that is located outside of the region shown in Fig. 3; see Fig. 1 for its location. If the direction of the electron flow through the graphene nanostructure is reversed, so that electrons flow instead from current contact 2 to current contact 1 (in Fig. 1), then the valley velocity field becomes strongest near current contact 2 and voltage contact 2, i.e., near the opposite edge of the sample to that where the valley velocity field is strongest in Fig. 3. For electron flow from current contact 2 to current contact 1, the direction of the valley velocity field is from right to left, i.e., its direction is opposite to that in Fig. 3, consistent with the chiral character of the valley current.

The chiral nature of the valley current is further clarified in Fig. 4. Figure 4(a) shows the strongest part of the valley velocity field associated with electron injection into a graphene nanostructure with broken inversion symmetry via a single interior carbon atom (colored orange) of the nanostructure, as

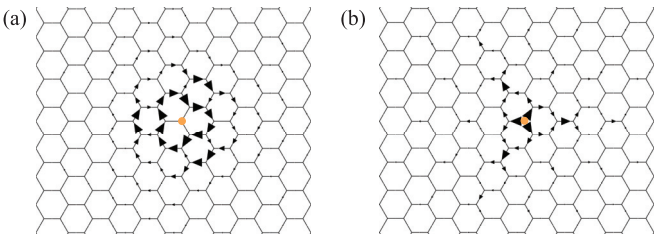

FIG. 4. (Color online) (a) Valley velocity field [Eq. (16)] and (b) velocity field [Eq. (15)] for electrons injected into a graphene nanostructure with broken inversion symmetry via a single carbon atom (orange). Only a small part of the graphene nanostructure is shown. $\Delta = 0.0602$ eV. $E_F = 0$.

in an idealized STM setup. The valley velocity field forms a vortex circulating clockwise (counterclockwise if the sign of Δ is changed) around the injection point, whereas the electron flux travels outwards overall from the injection point, as shown in Fig. 4(b).

In the vicinity of a contact, the valley current is due almost entirely to electrons injected into the nanostructure from that contact. This is true even for the voltage contact (Fig. 3) through which no *net* electric current flows since the zero net current is due to equal fluxes of electrons entering and leaving the contact. The valley current of electrons leaving the contact is much larger than that of those entering the contact. Thus a contact through which no net electric current flows can be used to create a valley current into a graphene nanostructure with broken inversion symmetry, i.e., it can, in principle, generate a pure valley current.

The results presented above have been for a graphene nanostructure with only armchair edges. Similar calculations for a rectangular structure of similar size (dimensions 9.656×9.838 nm) and similar contacts, but with two zigzag and two armchair edges, were carried out and yielded qualitatively similar results, but the effects of inversion symmetry breaking were found to be much stronger in this case: The nonlocal resistance for $\Delta = 0.0602$ eV was found to exceed that for $\Delta = 0$ by more that a factor of 100 for E_F near the Dirac point energy. Also, at its maximum, the valley current in the x direction was found to exceed the total conventional electric current through the nanostructure by a factor of more than 18. These large numbers are attributable to the flat electronic dispersion at graphene zigzag edges [31] in tight-binding models described by the noninteracting electron Hamiltonian (3). However, theoretical studies have suggested that electron-electron interactions may give rise to magnetism at zigzag edges [32,33]. The potential implications of this for valley currents and nonlocal resistances are beyond the scope of the present paper.

Different approaches for realizing valley currents in graphene have also been proposed based on electric fields acting on electrons in the presence of Berry curvature [4], graphene point contacts with zigzag edges [34], electron scattering at the boundary between monolayer and bilayer graphene [35], electron scattering at a line defect in graphene [36], illumination of monolayer [37] or bilayer [38] graphene by circularly polarized radiation, optical injection of a pure valley current in graphene [39], and gate-induced valley filtering in bilayer graphene [40]. Strong valley

current polarizations, comparable to those obtained with the present approach for the structure having both zigzag and armchair edges, have been estimated for some of these approaches [34,36,38–40], albeit for models of infinite two-dimensional graphene or infinite graphene ribbons. Also, unlike in the present work, the spatial distribution of valley currents was not reported in the previous studies [4,34–38,40], and the effects of boundaries between the graphene and source and drain electrodes were not taken into account.

IV. CONCLUSIONS

The present work suggests an approach for creating valley currents in graphene with broken inversion symmetry that differs fundamentally from previous proposals [2,4–9,34–41]. As has been explained above, it follows from Büttiker-Landauer theory that in the linear response regime considered here, the transport properties of nanostructures are determined by electron scattering states calculated in the limit where the driving electric field has been sent to zero. Consequently, in the linear response regime, the acceleration of electrons by the driving electric field has no effect on multiterminal resistance coefficients or on $\vec{I}^{\rm val}/I$, i.e., the ratio of the valley current $\vec{I}^{\rm val}$ and the conventional electric current I passing through the nanostructure. Thus the valley currents discussed here are not due to electron acceleration in an electric field in the presence of Berry curvature, but instead are a direct consequence of nonadiabatic injection of electrons from a contact into the graphene. They are strongest for graphene with broken inversion symmetry in the tunneling regime when the Fermi energy is in the spectral energy gap around the Dirac point. Consequently, in this regime, these valley currents are strongest close to the graphene/contact boundary. They are chiral and can be very strong close to the Dirac point, i.e., several times larger than the conventional electric current even after averaging over the entire graphene nanostructure. They can appear even at a voltage contact through which no *net* conventional electric current flows, provided that electrons are being emitted (and absorbed) by that contact. They are predicted to be realized whenever electrons cross into the graphene at an abrupt boundary (which may be regular or rough on the atomic scale) between a contact and graphene with broken inversion symmetry at energies in the spectral gap around the Dirac point. At Fermi energies well away from the Dirac point (i.e., outside of the gap in the density of states of the nanostructure), valley currents can still be induced by bias voltages applied to the nanostructure, but in this regime they are considerably weaker, are not sensitive to whether or not the inversion symmetry of the graphene is broken, and are not confined to regions of the nanostructure that are close to contacts. The fact that valley currents can be induced in graphene nanostructures even in the absence of inversion symmetry breaking has been recognized previously [34], and is a consequence of the fact that the Bloch state wave vector need not be a conserved quantity in nanostructures whose translational crystal symmetries are broken due to the presence of boundaries.

ACKNOWLEDGMENTS

This research was supported by NSERC, CIFAR, Westgrid, and Compute Canada.

[1] P. R. Wallace, Phys. Rev. **71**, 622 (1947).
[2] For a pedagogical review of the Berry phase and related topics, see D. Xiao, M.-C. Meng, and Q. Niu, Rev. Mod. Phys. **82**, 1959 (2010).
[3] T. Ando, T. Nakanishi, and R. Saito, J. Phys. Soc. Jpn. **67**, 2857 (1998).
[4] D. Xiao, W. Yao, and Q. Niu, Phys. Rev. Lett. **99**, 236809 (2007).
[5] R. Karplus and J. M. Luttinger, Phys. Rev. **95**, 1154 (1954).
[6] M. C. Chang and Q. Niu, Phys. Rev. Lett. **75**, 1348 (1995).
[7] M. C. Chang and Q. Niu, Phys. Rev. B **53**, 7010 (1996).
[8] Y. D. Chong, Phys. Rev. B **81**, 052303 (2010).
[9] R. V. Gorbachev, J. C. W. Song, G. L. Yu, A. V. Kretinin, F. Withers, Y. Cao, A. Mishchenko, I. V. Grigorieva, K. S. Novoselov, L. S. Levitov, and A. K. Geim, Science **346**, 448 (2014).
[10] G. Giovannetti, P. A. Khomyakov, G. Brocks, P. J. Kelly, and J. van den Brink, Phys. Rev. B **76**, 073103 (2007).
[11] B. Sachs, T. O. Wehling, M. I. Katsnelson, and A. I. Lichtenstein, Phys. Rev. B **84**, 195414 (2011).
[12] M. Kindermann, B. Uchoa, and D. L. Miller, Phys. Rev. B **86**, 115415 (2012).
[13] J. C. W. Song, P. Samutpraphoot, and L. S. Levitov, arXiv:1404.4019.
[14] M. Büttiker, Phys. Rev. Lett. **57**, 1761 (1986).
[15] S. Reich, J. Maultzsch, C. Thomsen, and P. Ordejón, Phys. Rev. B **66**, 035412 (2002).
[16] For a review, see G. Kirczenow and S. Ihnatsenka, in *Graphene Nanoelectronics: Metrology, Synthesis, Properties and Applications*, edited by H. Raza (Springer, Heidelberg, 2012), Chap. 13.
[17] H. Dalgleish and G. Kirczenow, Phys. Rev. B **72**, 155429 (2005); Nano Lett. **6**, 1274 (2006); Phys. Rev. B **73**, 245431 (2006); **73**, 235436 (2006).
[18] J. Buker and G. Kirczenow, Phys. Rev. B **72**, 205338 (2005); **78**, 125107 (2008).
[19] G. Kirczenow, P. G. Piva, and R. A. Wolkow, Phys. Rev. B **72**, 245306 (2005); **80**, 035309 (2009).
[20] G. Kirczenow, Phys. Rev. B **75**, 045428 (2007).
[21] P. G. Piva, R. A. Wolkow, and G. Kirczenow, Phys. Rev. Lett. **101**, 106801 (2008).
[22] D. M. Cardamone and G. Kirczenow, Phys. Rev. B **77**, 165403 (2008); Nano Lett. **10**, 1158 (2010).
[23] G. Kirczenow, in *The Oxford Handbook of Nanoscience and Technology, Volume I: Basic Aspects*, edited by A. V. Narlikar and Y. Y. Fu (Oxford University Press, Oxford, 2010), Chap. 4.
[24] F. Demir and G. Kirczenow, J. Chem. Phys. **134**, 121103 (2011).
[25] F. Rostamzadeh Renani and G. Kirczenow, Phys. Rev. B **84**, 180408(R) (2011); **85**, 245415 (2012); **87**, 121403(R) (2013).
[26] F. Demir and G. Kirczenow, J. Chem. Phys. **136**, 014703 (2012).

[27] F. Demir and G. Kirczenow, J. Chem. Phys. **137**, 094703 (2012).
[28] A. Saffarzadeh and G. Kirczenow, Appl. Phys. Lett. **102**, 173101 (2013).
[29] S. Majumder, B. Kardasz, G. Kirczenow, A. Spring Thorpe, and K. L. Kavanagh, Semicond. Sci. Technol. **28**, 035003 (2013).
[30] A. Saffarzadeh, F. Demir, and G. Kirczenow, Phys. Rev. B **89**, 045431 (2014).
[31] K. Nakada, M. Fujita, G. Dresselhaus, and M. S. Dresselhaus, Phys. Rev. B **54**, 17954 (1996).
[32] M. Fujita, K. Wakabayashi, K. Nakada, and K. Kusakabe, J. Phys. Soc. Jpn. **65**, 1920 (1996).
[33] For a recent review and further references, see J. L. Lado, N. García-Martínez, and J. Fernández-Rossier, arXiv:1502.07112.
[34] A. Rycerz, J. Tworzydlo, and C. W. J. Beenakker, Nat. Phys. **3**, 172 (2007).
[35] T. Nakanishi, M. Koshino, and T. Ando, Phys. Rev. B **82**, 125428 (2010).
[36] D. Gunlycke and C. T. White, Phys. Rev. Lett. **106**, 136806 (2011).
[37] T. Oka and H. Aoki, Phys. Rev. B **79**, 081406(R) (2009).
[38] D. S. L. Abergel and T. Chakraborty, Appl. Phys. Lett. **95**, 062107 (2009).
[39] L. E. Golub, S. A. Tarasenko, M. V. Entin, and L. I. Magarill, Phys. Rev. B **84**, 195408 (2011).
[40] D. R. da Costa, A. Chaves, S. H. R. Sena, G. A. Farias, and F. M. Peeters, Phys. Rev. B **92**, 045417 (2015).
[41] W. Yao, D. Xiao, and Q. Niu, Phys. Rev. B **77**, 235406 (2008).